E3-2014-92

J. Adam [1,6,*], A. A. Baldin [1,2], V. Chilap [3],
W. Furman [1], K. Katovsky [4], J. Khushvaktov [1], V. Kumar [5],
V. Pronskikh [1,7], I. Mar'in [1], A. Solnyshkin [1], M. Suchopar [6],
V. Tsoupko-Sitnikov [1], S. Tyutyunnikov [1], J. Vrzalová [1],
V. Wagner [6], L. Závorka [1]

MEASUREMENT OF THE HIGH-ENERGY NEUTRON FLUX ON THE SURFACE OF THE NATURAL URANIUM TARGET ASSEMBLY **QUINTA** IRRADIATED BY DEUTERONS OF 4- AND 8-GeV ENERGY

[1] Joint Institute for Nuclear Research, Dubna
[2] Institute for Advanced Studies "OMEGA", Dubna, Russia
[3] CPTP "Atomenergomash", Moscow
[4] University of Technology, Brno, Czech Republic
[5] G. G. S. Indraprastha University, New Delhi, India
[6] NPI, Rez near Praha, Czech Republic
[7] Fermi National Accelerator Laboratory, Batavia, USA
[*] E-mail: iadam@jinr.ru

Адам И. и др.   E3-2014-92

Измерение спектра нейтронов высокой энергии на поверхности мишени
из натурального урана установки КВИНТА, облучаемой дейтронами
с энергией 4 и 8 ГэВ

Анализируются результаты экспериментов на установке КВИНТА с мишенью из натурального урана, облученной на нуклотроне Объединенного института ядерных исследований дейтронами с энергией 4 и 8 ГэВ. Радиоактивные образцы ^{129}I, ^{232}Th, ^{233}U, ^{235}U, ^{nat}U, ^{237}Np, ^{238}Pu, ^{239}Pu и ^{241}Am были установлены на поверхности установки КВИНТА и облучались вторичными нейтронами. Нейтронный поток через РА-образцы мониторировался Al-фольгами. Скорость реакций ^{27}Al(n, y_1) ^{24}Na, ^{27}Al(n, y_2) ^{22}Na и ^{27}Al(n, y_3) ^{7}Be с эффективными порогами энергий 5, 27 и 119 МэВ измерялась при обеих энергиях дейтронов 4 и 8 ГэВ. Определены средние потоки нейтронов между эффективными пороговыми энергиями и эффективными границами спектров нейтронов (которые составляют 800 и 1000 МэВ для энергий 4 и 8 ГэВ). За счет отношения средних потоков нейтронов обнаружен очевидный сдвиг интенсивности нейтронных спектров в область больших энергий с увеличением энергии дейтронов от 4 до 8 ГэВ. Скорости реакций и средние нейтронные потоки рассчитывались программами MCNPX2.7 и MARS15.

Adam J. et al.   E3-2014-92

Measurement of the High-Energy Neutron Flux on the Surface
of the Natural Uranium Target Assembly QUINTA Irradiated by Deuterons
of 4- and 8-GeV Energy

Experiments with a natural uranium target assembly QUINTA exposed to 4- and 8 GeV deuteron beams of the Nuclotron accelerator at the Joint Institute for Nuclear Research (Dubna) are analyzed. The ^{129}I, ^{232}Th, ^{233}U, ^{235}U, ^{nat}U, ^{237}Np, ^{238}Pu, ^{239}Pu and ^{241}Am radioactive samples were installed on the surface of the QUINTA set-up and irradiated with secondary neutrons. The neutron flux through the RA samples was monitored by Al foils. The reaction rates of ^{27}Al(n, y_1) ^{24}Na, ^{27}Al(n, y_2) ^{22}Na and ^{27}Al(n, y_3) ^{7}Be reactions with the effective threshold energies of 5, 27 and 119 MeV were measured at both 4- and 8-GeV deuteron beam energies. The average neutron fluxes between the effective threshold energies and the effective ends of the neutron spectra (which are 800 or 1000 MeV for energy of 4- or 8-GeV deuterons) were determined. The evidence for the intensity shift of the neutron spectra to higher neutron energies with the increase of the deuteron energy from 4 to 8 GeV was found from the ratios of the average neutron fluxes. The reaction rates and the average neutron fluxes were calculated with MCNPX2.7 and MARS15 codes.

INTRODUCTION

For transmutation of long-lived radioactive nuclides of nuclear waste one of the possible methods is to apply intense spallation neutron source [1–4]. World over a large number of research and development programs related to accelerator operated neutron sources have been invoked in this direction, e.g., RACE [5] in USA, J-PARC [6] in Japan, ADS program of India [7] and China [8], MYRRHA in Belgium [9], SINQ at PSI [10] , PNF in South Korea [11], n-ToF at CERN [12] and the quasi mono-energetic neutron sources at the TSL, Uppsala [13] and NPI, Řež [14].

At JINR, Dubna, during the last two decades in the framework of "Energy + Transmutation of Radioactive Waste (E + T RAW)" projects, the extensive ADS studies had been carried out with use of high-energy proton and deuteron beams. In particular, the transmutation rates of both long-lived fission products (LLFP) and trans-uranium (LLTRU) nuclides had been measured in the neutron fields generated within the lead–uranium [15, 16] and lead–graphite [17] targets with moderators, as well as in the natural uranium target assembly (TA) QUINTA (with and without the lead blanket) [18] irradiated by deuterons of energy 1–8 GeV. The effective incineration of LLFP and LLTRU needs a maximally hard neutron spectrum due to the high thresholds of (n, f) and (n, xn) reactions necessary for its transmutation. Just such a neutron spectrum is realized for TA QUINTA. So, it is important to clarify the dependence of its shape on incident deuteron energy E_d to define the optimal value E_d.

As the activation cross section of a particular nuclide for a nuclear reaction is a strong function of neutron energy, therefore determination of differential neutron fluence as a function of energy is highly desirable. For determination of the neutron flux corresponding to neutron energy cross sections, library of several monitor reactions [19, 20] is either available or it can be produced from a simulation code like CASCADE [21, 22] or TALYS [23]. For unfolding of the neutron flux in a range of energy, two methods have been used. In the first method, activation cross section in the given energy range is considered to be constant and in the second method, where activation cross sections are available in the energy range, neutron flux then has been considered as independent of energy. In both cases, neutron flux is estimated by knowing the reaction rate from an experiment [24].

1

In the present work, this problem is studied measuring by an activation method [24] the yields of the product nuclei in $^{27}\text{Al}\,(n, y_1)\,^{24}\text{Na}$, $^{27}\text{Al}\,(n, y_2)\,^{22}\text{Na}$ and $^{27}\text{Al}\,(n, y_3)\,^{7}\text{Be}$ reactions having the threshold neutron energies $E_{n\,\text{th}} = 3.25$, 24.3 and 68.1 MeV, respectively. These three monitor reactions have been considered for measurement of the flux of spallation neutrons produced in 2-, 4- and 8-GeV deuteron colliding with the uranium target of QUINTA. The effective threshold energies are estimated (see, Sec. 3 for details) as $E_{\text{eff\,th}} = 5$, 27 and 119 MeV for ^{24}Na, ^{22}Na and ^{7}Be nuclides, so it becomes possible to get the information on high-energy tale ($E_n \geqslant 120$ MeV) of neutron spectrum in such a fast deep subcritical multiplying system as TA QUINTA. The results of these measurements are compared with our calculations by MCNPX2.7 and MARS15 codes to estimate their ability to reproduce the whole shape of neutron spectra.

Here, it is appropriate to note that in [18] the (n, γ), (n, f) and $(n, 2n)$ reactions for ^{232}Th and ^{238}U samples placed in TA QUINTA were studied in the E_d range (2–8) GeV. The results showed no dependence (in the limits of experimental uncertainties) of the ratios of these reaction rates on incident deuteron energy. This means that up to $E_n \approx 7$ MeV the shape of the neutron spectra under consideration retains practically unchanged. So, the present work can significantly improve the existing information on the neutron field in TA QUINTA.

1. EXPERIMENTAL SET-UP AND MEASUREMENTS OF DEUTERON BEAM INTENSITY

The target assembly QUINTA consists of four identical sections of hexagonal aluminum containers with an inscribed circular diameter of 284 mm, each of which contains 61 cylindrical metallic natural uranium rods. Each rod of 36 mm in diameter and 104 mm length weighs 1.72 kg and is wrapped in Al shell. Total mass of uranium in one section is 104.92 kg. The front fifth section has the cylindrical input beam channel of diameter 8 cm and consists of 54 uranium rods. Thus, the total mass of uranium in the target assembly is 512.56 kg. The uranium target is surrounded by lead blanket of 10 cm thick.

In Fig. 1, a outer thick Pb shielding is shown with a beam window and the additional one designed to accommodate experimental samples. Figure 1, b represents a top view on the horizontal cut (in a beam plane) of TA.

The sample box is located on a lateral surface of the lead blanket in special window of size 50×150 mm perpendicular to the beam direction. The center of the sample window lies on symmetry axis of the third section of TA QUINTA as shown in Fig. 1, b. After putting the radioactive samples ^{129}I, ^{232}Th, ^{233}U, ^{235}U, $^{\text{nat}}\text{U}$, ^{237}Np, ^{238}Pu, ^{239}Pu and ^{241}Am with adjacent Al monitor in 3×3 matrix arrangement in the sample window it is plugged with 100 mm thick lead (see Fig. 1, c).
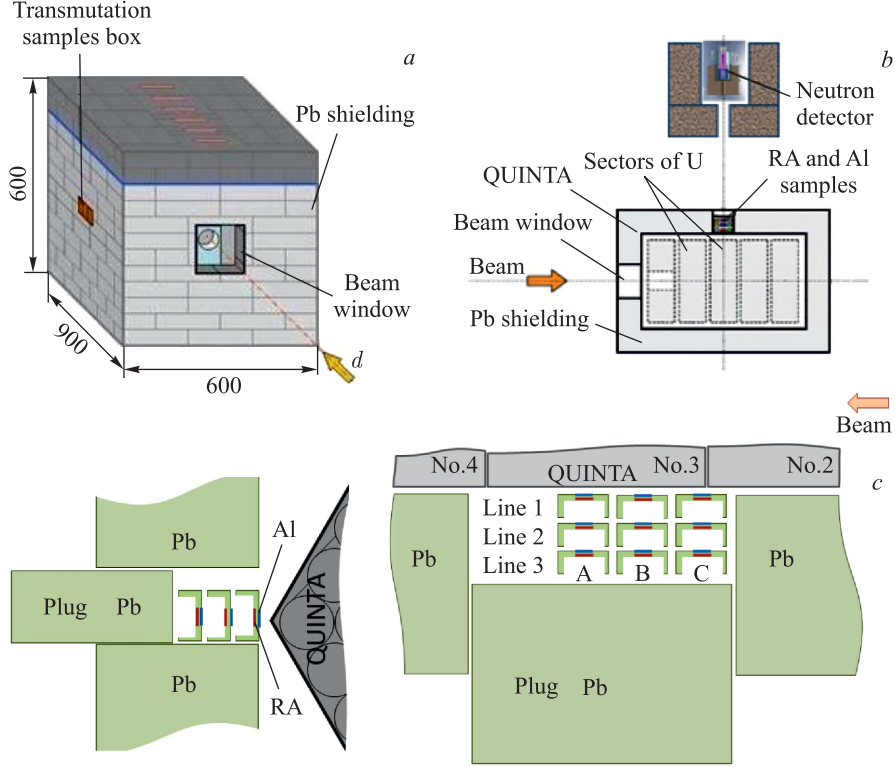
Fig. 1. *a*) The general view of TA QUINTA; *b*) a top view of the horizontal cut of TA QUINTA showing replacement of experimental samples; *c*) enlarged view of sample window carrying Al monitors with adjacent RA samples in 3×3 matrix. The lead plug of sizes $150 \times 100 \times 50$ mm is also shown

The QUINTA set-up was directly irradiated by deuteron with energies 2, 4, and 8 GeV at the Nuclotron accelerator in December 2012 during 376, 561, and 970 min, respectively. Neutrons were produced by way of spallation, fission and evaporation processes after $d + {}^{\mathrm{nat}}\mathrm{U}$ collisions.

The ${}^{27}\mathrm{Al}\,(d, y_1)\,{}^{24}\mathrm{Na}$ reaction in the Al monitors was used to determine the integral number of deuterons impinging on the set-up. The reaction cross sections at 2-, 4-, and 8-GeV deuteron energies E_d were found by fitting the experimental data from EXFOR library [19] for the range E_d (65–80) MeV, and their experimental values 15.25(150) mb at 2.33 GeV [25], 14.1(13) mb at 6.0 GeV [26], and 14.7(12) mb at 7.3 GeV [26] are used (see Fig. 2, where the low-energy experimental values with unknown uncertainties and those less than 10 mb were omitted). Four different fits were made: the first with 4 points from
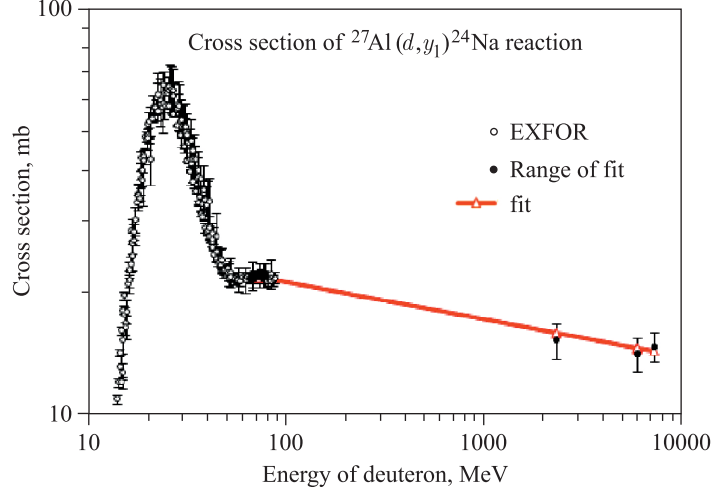
3

Fig. 2. Experimental data and fit of cross section of $^{27}\mathrm{Al}\,(d,y_1)\,^{24}\mathrm{Na}$ reaction. For low-energy deuterons the range of fit is from 65 up to 80 MeV

the energy range between 70 and 75 MeV, the second with 14 points between 65 and 80 MeV, the third with 24 points between 60 and 85 MeV, and the fourth with 31 points with the deuteron energies between 55 and 89 MeV. In addition, three cross sections for the energies higher than 2.3 GeV were used in all four fits.

In fitting there was assumed that the cross section (CS) depends linearly in the log–log scale on deuteron energy, i.e., $\mathrm{CS} = \exp{(a_0 + a_1 \ln E_d)}$. The smallest $\chi^2 = 0.10$ has been found for the second fit, but it is not significantly different from the first and third ones. The fourth fit gives $\chi^2 = 0.21$. The errors of the fitted cross sections are 1.62% at the deutron energy of 2 GeV and 2.06% at 8 GeV. The differences between the fitted cross sections for the second and fourth sets of experimental data (as described above) are 0.27 mb at 2 GeV and 0.38 mb at 8 GeV, respectively. These differences in cross sections between the second and fourth fits were accepted as the systematic errors and were added to the uncertainties of fitted cross sections presented in the fifth column of Table 1.

Table 1. The production rates $Q(^Z\mathrm{A})$ of $^{24}\mathrm{Na}$, $^{22}\mathrm{Na}$ and $^7\mathrm{Be}$ isotopes in the Al beam monitors at measured deuteron energies and the cross sections of the respective reactions $^{27}\mathrm{Al}\,(d,y_i)\,^Z\mathrm{A}$

Beam energy	$Q(^{24}\mathrm{Na})$	$Q(^{22}\mathrm{Na})$	$Q(^7\mathrm{Be})$	$\sigma(^{24}\mathrm{Na})$, mb	$\sigma(^{22}\mathrm{Na})$, mb	$\sigma(^7\mathrm{Be})$, mb
2 GeV	3263(16)	3912(36)	2804(19)	16.0 (4)	19.2 (5)	13.8(4)
4 GeV	3441(30)	4080(25)	3708(21)	15.0 (4)	17.8 (6)	15.2(5)
8 GeV	1167(7)	1386(19)	1436(9)	14.1 (5)	16.8(6)	17.4(6)

4

In the course of Al beam monitor analysis for ^{24}Na, the product reaction rates of ^{22}Na and ^{7}Be in the reactions ^{27}Al(d, y_2) ^{22}Na and ^{27}Al(d, y_3) ^{7}Be were also determined. The measured production rate, Q, of ^{24}Na, ^{22}Na, and ^{7}Be is given in Table 1. The ratios of the measured values for 2-, 4- and 8-GeV beam energies are $Q(^{22}\text{Na})/Q(^{24}\text{Na}) = 1.199(13)$, $1.186(13)$, and $1.188(18)$; and $Q(^{7}\text{Be})/Q(^{24}\text{Na}) = 0.859(7)$, $1.078(11)$, and $1.231(18)$. It should be noted that these ratios are equal to the corresponding cross-section ratios, $\sigma(^{22}\text{Na})/\sigma(^{24}\text{Na})$ and $\sigma(^{22}\text{Na})/\sigma(^{24}\text{Na})$. Such cross-section ratios for ^{22}Na and ^{7}Be product nuclei are also given in Table 1.

Using the measured rates of ^{27}Al(d, y_1) ^{24}Na reaction obtained via study of deuteron beam monitoring and the fitted cross sections, we obtained the integral beam intensities at 2-, 4-, and 8-GeV deuteron energies 3.02(10)E+13, 2.73(10)E+13 and 9.1(4)E+12, respectively.

2. NEUTRON MONITORS OF THE RADIOACTIVE SAMPLES, EXPERIMENTAL RESULTS

The neutron fluxes through irradiated radioactive samples were monitored by the Al foils with diameter 21 mm placed close to the every RA sample. The weight of monitoring Al foil was about 0.1 g in the first experimental run 'a', when energy of deuterons was 2 GeV. The activities of these foils after irradiation by spallation neutrons were not enough to yield results with required accuracy. Then, in the second experiment 'b' with beam energy 4 GeV and in the third experiment 'c' with beam energy 8 GeV, monitor Al foils with diameter 21 mm and thickness about 1.5 mm were used. Their weights were measured with accuracy of 0.02% and the average value is 1.3264(9) g. Positions of Al monitors are shown in Fig. 1, c. Here, nine sandwiches composed of Al-monitor foils and the adjacent RA samples (referred to below as Al^{Z}A) were allocated in three layers and three columns marked as A, B and C (also, see Tables 3 and 4).

Two sets of three foils, namely, Al$^{\text{nat}}$Ub $+$ Al^{232}Thb $+$ Al^{237}Npb are measured in experiment with 4 GeV, and Al$^{\text{nat}}$Uc $+$ Al^{232}Thc $+$ Al^{233}Uc in experiment with 8-GeV beam. The weight of three foils is 3.9715(27) g in experiment 'b' and 3.9776(27) g in experiment 'c', respectively. First set is measured for 26.7 d and the second set for 14.9 d in order to receive enough accuracy of the reaction rates of ^{27}Al(n, y_2) ^{22}Na (T$_{1/2}$ of ^{22}Na being 2.6019 y) and ^{27}Al(n, y_3) ^{7}Be (T$_{1/2}$ of ^{7}Be being 53.29 d) reactions. This was chosen taking into account the expected less neutron fluxes for these reactions.

The reaction rate R is defined as the number of produced residual nuclei per atom of the sample, per incident deuteron and per second. A number of produced residual nuclei are established by measuring their emitted γ-rays with the HPGe detector. To analyze γ-ray spectra we determine a position and an area of peak by means of an interactive program of DEIMOS [27].

The energy and efficiency calibrations for four spectrometers used in the measurements were performed separately. The corrections for self-absorption of γ-rays for one Al foil are less than 1.7% or 5.3% for the set of three foils for gamma of energy $E_\gamma = 477$ keV. The values E_γ and the intensities of γ transitions per decay (I_γ) are determined with high accuracy and the results are also presented in Table 2. The correction for coincidence of cascade γ-rays depends on the detector efficiency, ε_γ and the intensity I_γ. The data for all four used detectors are shown in Table 2. The coincidence correction $\sim 41\%$ is the largest for ^{22}Na for the OrtecNew2 detector. The correction of changing intensity of deuteron beam is negligibly small, i.e., less than 1% for the experiments and three residual nuclei, except in case of irradiation with $E_d = 8$ GeV beam and ^{24}Na residual nuclide where the correction is 0.911. For the details of measurements and analysis of gamma spectra of activation detectors, see references [15, 17].

The reaction rates for ^{27}Al$(n, x\gamma_1)\,^{24}$Na reaction measured at $E_d = 4$ and 8 GeV and the respective calculated values are given in Tables 3 and 4, correspondingly. The average values of R for monitors placed in parallel layers 1, 2 and 3 or perpendicular columns to beam A, B and C are given also in Tables 3 and 4. It can be noted that there is a slight tendency of decrease of R value for any monitor when its distance from the beam axis increases. This effect is very clearly seen in case of data in Table 3. The maximum value of R is observed for the central group of monitors placed in B column. The overall average values $\langle R \rangle$ for all monitors in 4- and 8-GeV experiments are determined to be 7.5(4)E-29 and 12.2(7)E-29, respectively. These values go up with incident energy because of the increase in the intensity of the neutron flux defined in turn by almost linear growth of neutron multiplicity observed in [18]. A comparison of the experimental reaction rates and the respective values calculated by MCNPX2.7 code demonstrated rather good agreement for $E_d = 4$ GeV and the satisfactory one for $E_d = 8$ GeV. But using MARS15 code leads to the experiment/calculation ratios between 2.3 and 5.

Note, that the analysis and results of the reaction rates for RA samples ^{129}I, ^{232}Th, ^{233}U, ^{235}U, $^{\text{nat}}$U, ^{237}Np, ^{238}Pu, ^{239}Pu and ^{241}Am will be published elsewhere.

The reaction rates $\langle R \rangle$ for the product nuclei ^{22}Na and ^{7}Be were obtained in the same way as described above for ^{24}Na. All three measured reaction rates $\langle R \rangle$ together with their uncertainties and the respective calculated values are given in Table 5.

An analysis of the data represented in Table 5 leads to very important conclusions on the dependence of the shape of the neutron spectrum of the incident energy. Indeed, if the ratio $\langle R \rangle (8 \text{ GeV})/\langle R \rangle (4 \text{ GeV})$ for ^{24}Na having a low-reaction threshold is less than two, so for ^{22}Na and ^{7}Be product nuclei with much higher thresholds these ratios reach about 5 and 7, correspondingly. It gives evi-

Table 2. The coincidence corrections at the second position of the monitors. The E_γ and I_γ values are taken from [28, 29]. The relative efficiencies of gamma detection shown in the second column are given for $E_\gamma = 1332$ keV

Gamma detector	Relative efficiency	Coincidence corrections		
		^{24}Na [28]		^{22}Na [29]
		$E_\gamma =$ $= 1368.626(5)$ keV $I_\gamma = 99.9935(5)\%$	$E_\gamma =$ $= 2754.007(11)$ keV $I_\gamma = 99.872(8)\%$	$E_\gamma =$ $= 1274.537(7)$ keV $I_\gamma = 99.94(3)\%$
A-Canberra	18.9%	1.08	1.11	1.19
B-OrtecOld	27.7%	1.15	1.19	1.29
C-OrtecNew2	32.9%	1.25	1.29	1.41
D-OrtecNew1	28.3%	1.16	1.19	1.26

Note. There are no coincidence summing corrections for decay of ^{7}Be. The production rates for this isotope were calculated using values $E_\gamma = 477.6035(20)$ keV and $I_\gamma = 10.44(4)\%$ [30].

Table 3. The reaction rates R of ^{27}Al (n, y_1) ^{24}Na reaction measured at $E_d = 4$ GeV in units of E-29/atom/deuteron/s in three layers and A, B, and C columns. The calculated values marked as 'a' and 'b' were obtained using MCNPX2.7 [31] and MARS15 [32] codes, respectively

Layers	Position of monitor			Average of lines
	A	B	C	
Layer 1	Al^{235}Ub	Al^{238}Pub	Al^{129}Ib	
exp	—		8.8(6)	8.8(6)
calc$^{(a)}$	8.57	9.55	8.68	
exp/calc$^{(a)}$	—		1.01(6)	
calc$^{(b)}$	1.62(12)	1.81(13)	2.08(16)	
exp/calc$^{(b)}$			4.2(4)	
Layer 2	Al^{241}Amb	Al^{233}Ub	Al^{237}Npb	
exp	—	9.0(3)	7.5(3)	8.3(7)
calc$^{(a)}$	8.12	8.57	7.46	
exp/calc$^{(a)}$	—	1.05(4)	1.01(5)	
calc$^{(b)}$	1.71(14)	1.80(16)	1.52(13)	
exp/calc$^{(b)}$		5.0(4)	5.0(5)	
Layer 3	Al^{232}Thb	Al^{239}Pub	Al^{nat}Ub	
exp	7.4(5)	7.8(5)	6.51(22)	6.8(4)
calc$^{(a)}$	7.40	7.70	6.63	
exp/calc$^{(a)}$	0.99(6)	1.01(6)	0.98(3)	
calc$^{(b)}$	1.48(11)	2.11(13)	1.56(14)	
exp/calc$^{(b)}$	5.0(5)	3.7(3)	4.2(4)	
Average of columns	7.4(5)	8.6(5)	7.0(5)	

Layers	Position of monitor			Average of lines
	A	B	C	
Layer 1	Al^{nat}Uc	Al^{129}Ic	Al^{239}Puc	
exp	12.5(6)	13.6(9)	15.3(9)	13.4(8)
calc$^{(a)}$	18.5	18.8	17.1	
exp/calc$^{(a)}$	0.68(3)	0.72(5)	0.90(5)	
calc$^{(b)}$	4.3(3)	4.9(5)	6.6(4)	
exp/calc$^{(b)}$	2.90(25)	2.8(3)	2.31(19)	
Layer 2	Al^{235}Uc	Al^{233}Uc	Al^{238}Puc	
exp	13.6(11)	13.5(8)	11.5(5)	12.3(7)
calc$^{(a)}$	17.0	16.7	14.6	
exp/calc$^{(a)}$	0.80(6)	0.81(5)	0.79(4)	
calc$^{(b)}$	5.44(11)	4.8(3)	4.9(4)	
exp/calc$^{(b)}$	2.5(5)	2.81(26)	2.33(20)	
Layer 3	Al^{232}Thc	Al^{241}Amc	Al^{237}Npc	
exp	10.4(6)	—	11.4(9)	10.7(5)
calc$^{(a)}$	15.1	15.1	12.9	
exp/calc$^{(a)}$	0.69(4)	—	0.83(4)	
calc$^{(b)}$	3.96(30)	5.7(5)	3.45(27)	
exp/calc$^{(b)}$	2.62(24)		3.32(36)	
Average of columns	11.7(9)	13.5(6)	12.8(12)	

dence that the neutron spectrum on the surface of TA QUINTA becomes "harder" with increase of incident energy.

Other essential conclusions are related to the inability of both used codes to reproduce the discussed above dependence of the high-energy tale of the neutron spectrum on incident energy.

As seen from Table 5, the calculated values of ratios $\langle R \rangle\,(8\,\text{GeV})/\langle R \rangle\,(4\,\text{GeV})$ are explicitly mismatched with the corresponding experimental ones, as for the code MCNPX2.7 these ratios lie in the range from 2.2 to 2.7 and for the MARS15 one — in the range from 2.1 to 3.

Note, in addition, that at 4-GeV deuteron energy for the effective thresholds $E_{\text{th eff}} \leqslant 27$ MeV the MCNPX2.7 code reproduces $\langle R \rangle$ values rather well, while for $E_{\text{th eff}} = 119$ MeV the disagreement reaches 2.5 times. In the case of 8-GeV deuteron energy for highest thresholds of ^{7}Be, the exp/(calc) ratio increases up to 6.4. For the MARS15 code the situation is much worse: the difference between experimental and calculated $\langle R \rangle$ values at $E_{\text{th eff}} = 119$ MeV reaches 18 and 41 times for the deuteron energies of 4 and 8 GeV, respectively. In general, this means that the used codes are not able to reproduce the high-energy

Table 5. A comparison of the experimental and calculated rates of ^{27}**Al** (n, y_1) ^{24}**Na,** ^{27}**Al** (n, y_2) ^{22}**Na and** ^{27}**Al** (n, y_3) ^{7}**Be reactions obtained for 4- and 8-GeV deuteron energies in units of E-29/atom/deuteron/s. The experimental errors are marked as** $d(R)$

Residual nuclei	Data	$E_d = 4$ GeV R[E-29]	$E_d = 8$ GeV R[E-29]	$R\,(8\text{ GeV})/R\,(4\text{ GeV})$
^{24}Na	exp	7.5(4)	12.2(5)	1.64(12)
	calc[a]	7.473	16.75	2.24
	calc[b]	1.76	4.66	2.64
	exp/calc[a]	1.00(6)	0.73(3)	
	exp/calc[b]	4.25(10)	2.63(12)	
^{22}Na	exp	0.522(29)	2.73(22)	5.2 (5)
	calc[a]	0.71	1.73	2.43
	calc[b]	0.61	1.32	2.16
	exp/calc[a]	0.73(4)	1.58(13)	
	exp/calc[b]	0.86(3)	2.07(17)	
^{7}Be	exp	0.069(11)	0.47(8)	6.8 (15)
	calc[a]	0.0274	0.0736	2.69
	calc[b]	0.0038	0.0114	3.00
	exp/calc[a]	2.5(4)	6.4(11)	
	exp/calc[b]	18.2(29)	41	

[a] Calculations were performed with code MCNPX2.7 [31].
[b] Calculations were performed with code MARS15 [32].

part of the neutron spectrum of TA QUINTA. And, moreover, the obtained results indicate instability in the transition from the code to the code.

3. ANALYSIS OF NEUTRON FLUX DATA

The results of the present measurements partly shown in Tables 3–5 allow one to extract the neutron fluxes for three intervals of neutron energy via the method described below.

The measured reaction rate R for the given product nucleus ^{Z}A created in ^{27}Al (n, y) ^{Z}A process is the convolution in energy E_n of the neutron flux $\phi[n/\text{cm}^2/\text{MeV}/\text{deuteron/s}]$ and the respective cross sections $\sigma_i(E_n)$ leading to the nucleus ^{Z}A:

$$R = \int_0^{E_n^{\max}} \sum_i \sigma_i(E_n)\,\phi(E_n)\,dE_n = \int_0^{E_n^{\max}} \sigma(E_n)\,\phi(E_n)\,dE_n. \qquad (1)$$

9

The integration in formula (1) is carrying out up to the maximal energy of the neutron spectrum. If the cross sections $\sigma_i(E_n)$ are known from experiment or calculations, it is possible, in principle, to deduce the flux $\phi(E_n)$ solving the integral equation (1). But in reality this is a very difficult task, especially in our case, when many reactions give contribution to a formation of the product nucleus.

In Fig. 3, the existing experimental data for the studied reactions taken from the EXFOR compilation [19] and calculated by the TALYS 1.4 code [23] are presented in function of neutron energy.

As follows from Fig. 2, the most contribution in the integral (1) defining the reaction rates for production of ^{24}Na and ^{7}Be nuclei gets from the neutron energy ranges (5–27) MeV and $(119-E^{\max})$ MeV referred below to as the first and the third ones. So, the production of ^{22}Na can be conditionally assigned to the energy
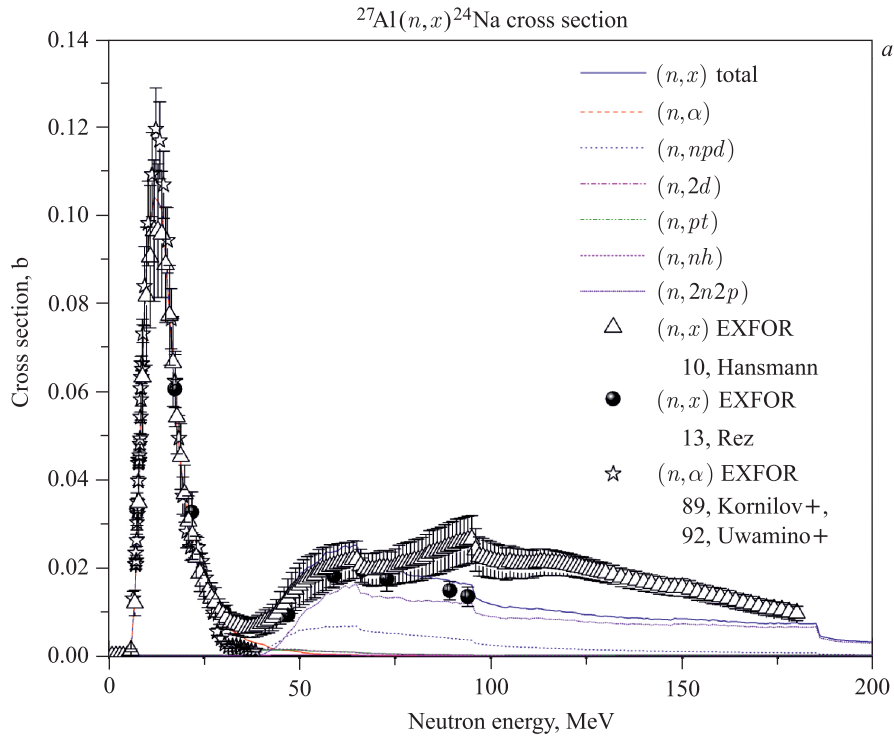

Fig. 3, *a*. The production cross section of ^{24}Na nucleus in $n + $ Al collisions up to $E_n = 200$ MeV calculated by the TALYS code [23] and compared with experimental data from the EXFOR library [19]
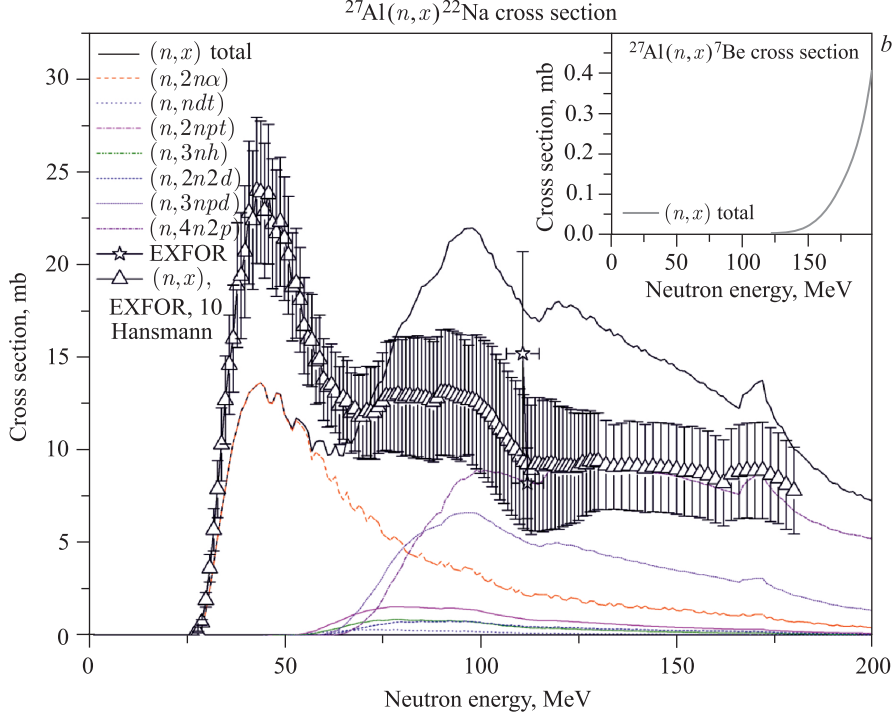
10

Fig. 3, *b*. The same as in Fig. 3, *a*, but for ^{22}Na and ^{7}Be nuclei

interval (27–119) MeV denoted below by index 2. So, for solving of Eq. (1) the following procedure used in [24] can be applied.

Assuming that the neutron flux $\phi_3(E)$ in the third energy interval is constant, and denoting this as ϕ_3, it is possible to express the reaction rate for ^{7}Be production as

$$R_3 = \int\limits_3^4 \sigma_3(E)\,\phi_3(E)\,dE \cong \phi_3 \sum_3^4 \sigma_3(E)\Delta E = \phi_3 X_{34}(3), \qquad (2)$$

where the limits of integration or summation are from 119 MeV up to $E^{\max}$, that is defined as a half of the deuteron energy or as the effective end of neutron spectrum (see below). The value $\sigma_3(E)$ denotes the sum of all cross sections leading to final nucleus ^{7}Be at neutron energy E and $X_{34}(3)$ represents the sum of $\sigma_3(E)$ over whole third energy interval. So, the neutron flux ϕ_3 may, therefore, be calculated as

$$\phi_3 = R_3/X_{34}(3). \qquad (3)$$

11

In the second neutron energy range, the reaction rate for ^{22}Na product nucleus could be written as follows:

$$R_2 = \phi_2 X_{23}(2) + \phi_3 X_{34}(2), \tag{4}$$

where as above it has been assumed that the neutron flux ϕ_2 is constant over the second energy interval. So, from (4) one obtains

$$\phi_2 = \{R_2 - \phi_3 X_{34}(2)\}/X_{23}(2). \tag{5}$$

At last, the reaction rate for ^{24}Na production is expressed as

$$R_1 = \phi_1 X_{12}(1) + \phi_2 X_{23}(1) + \phi_3 X_{34}(1), \tag{6}$$

that gives the neutron flux ϕ_1 in the form

$$\phi_1 = \{R_1 - \phi_2 X_{23}(1) - \phi_3 X_{34}(1)\}/X_{12}(1). \tag{7}$$

The unfolding of neutron spectra is started from data of the residual nuclei ^{7}Be, which have the highest value of threshold energy 68.1 MeV for reaction ^{27}Al(n, y_3) ^{7}Be, but significant value of cross section 1.06E-6 barn appears only at 119 MeV, denoted by '3'. Neutron flux ϕ_3 is then calculated from Eq. (3). The flux ϕ_2 from the threshold of 23.4 MeV of ^{27}Al(n, y_2) ^{22}Na reaction to the threshold energy '3' is again assumed to be constant. The respective part of the cross section $X_{32}(2)$ was calculated from 27 MeV (denoted by '2'), because the significant value 1.08E-5 barn of $\sigma_2(E)$ is approached just at neutron energy of 27 MeV. Neutron flux ϕ_2 was calculated with the help of Eq. (5). The neutron flux ϕ_1 between effective threshold 5 MeV (label '1'), where cross section is only 8.36E-6 barn and threshold '2' was taken constant and calculated from Eq. (7). In Fig. 3, the cross sections of these three reactions as a function of neutron energy are given. The cross sections were calculated from the TALYS code and are compared with experimental values from the EXFOR library, see Fig. 3.

Table 6. The sums of cross sections, X_{12}, X_{23} and X_{34} in barn

Product	X_{12}	X_{23}	$X_{34}^{\text{a)}}$	$X_{34}^{\text{b)}}$	$X_{34}^{\text{c)}}$	$X_{34}^{\text{d)}}$
^{24}Na	1.08(11)	1.69(20)	18.8(19)	37.7(47)	7.23(59)	9.20(75)
^{22}Na	—	1.23(15)	18.9(16)	36.4(41)	7.48(74)	9.48(67)
^{7}Be	—	—	8.11(113)	21.2(63)	1.72(20)	2.60(26)

Note. 1) Calculations were performed with the end of neutron spectrum $E^{\text{max}} = E_d/2$ — a) and b) for $E_d = 4$ and 8 GeV, respectively.

2) Calculations were performed with effective end of neutron spectrum E^{max} equivalent to 800 MeV c) and to 1000 MeV d) for $E_d = 4$ and 8 GeV, correspondingly.

To extract information about the neutron spectra following the procedure described above, one needs to obtain initially the relevant sums of the corresponding cross sections in all three energy intervals. The calculations of the sums of cross sections $X_{12}(1)$, $X_{23}(1)$ and $X_{23}(2)$ were performed with aid of experimental

Table 7. The deduced average neutron fluxes ϕ_i(exp) in the units [neutrons/cm^2/MeV/ deuteron/s] $\cdot$ 10^{-5} and their calculated values for the deuteron energies 4 and 8 GeV

Product nucleus	Fluxes or their ratios	$E_d = 4$ GeV	$E_d = 8$ GeV	$\phi(8$ GeV$)/\phi(4$ GeV$)$
^{24}Na	$\phi_1(\text{exp})^a$	4.7(8)	7.8(12)	1.66(38)
	$\phi_1(\text{exp})^b$	4.8(8)	8.1(13)	1.69(39)
	$\phi_1(\text{calc})^c$	5.160	12.91	2.50
	$\phi_1(\text{calc})^d$	5.885	11.71	1.99
	$\phi_1(\text{exp})^a/\phi_1(\text{calc})^c$	0.91(16)	0.60(9)	
	$\phi_1(\text{exp})^a/\phi_1(\text{calc})^d$	0.80(14)	0.67(10)	
	$\phi_1(\text{exp})^b/\phi_1(\text{calc})^c$	0.93(16)	0.63(10)	
	$\phi_1(\text{exp})^b/\phi_1(\text{calc})^d$	0.82(14)	0.69(11)	
^{22}Na	$\phi_2(\text{exp})^a$	0.29(6)	1.6(4)	5.3(6)
	$\phi_2(\text{exp})^b$	0.18(7)	0.83(35)	4.7(5)
	$\phi_2(\text{calc})^c$	0.261	0.550	1.11
	$\phi_2(\text{calc})^d$	0.525	1.007	1.92
	$\phi_2(\text{exp})^a/\phi_2(\text{calc})^c$	1.11(23)	2.9(7)	
	$\phi_2(\text{exp})^a/\phi_2(\text{calc})^d$	0.55(11)	1.6(4)	
	$\phi_2(\text{exp})^b/\phi_2(\text{calc})^c$	0.69(27)	1.5(6)	
	$\phi_2(\text{exp})^b/\phi_2(\text{calc})^d$	0.34(13)	0.82(35)	
^{7}Be	$\phi_3(\text{exp})^a$	0.0085(18)	0.022(8)	2.6(11)
	$\phi_3(\text{exp})^b$	0.040(8)	0.18(4)	4.5(14)
	$\phi_3(\text{calc})^c$	0.00271	0.00370	1.36
	$\phi_3(\text{calc})^d$	0.00899	0.00885	0.984
	$\phi_3(\text{exp})^a/\phi_3(\text{calc})^c$	3.1(7)	6.0(21)	
	$\phi_3(\text{exp})^a/\phi_3(\text{calc})^d$	0.94(20)	2.5(9)	
	$\phi_3(\text{exp})^b/\phi_3(\text{calc})^c$	14.8(30)	4.9(11)	
	$\phi_3(\text{exp})^b/\phi_3(\text{calc})^d$	4.4(9)	20(5)	

[a] The values ϕ_3(exp) were deduced with ends of neutron spectra $E^{\max} = 2$ or 4 GeV for $E_d = 4$ or 8 GeV, correspondingly.

[b] The values ϕ_3(exp) were deduced with the effective ends of neutron spectra $E^{\max} = 800$ or 1000 MeV for $E_d = 4$ or 8 GeV, correspondingly.

[c] Calculations were performed with code MCNPX2.7 [34].

[d] Calculations were performed with code MARS15 [35, 36].

data from EXFOR 10, Hansmann, see Fig. 3. The parts of sums $X_{34}(3)$ for neutron energy range (119–200) MeV were calculated using the deterministic code TALYS 1.4 [23]. But for $E_n > 200$ MeV, where the TALYS code is not applicable, the $X_{34}(i)$ values were obtained in the following manner. It was assumed that for these energies the cross sections for production of the considered nuclei are the same for incident neutrons and protons. Using our experimental results [31] for the respective cross sections received with 660 MeV protons and the results of [32, 33] measured at 2- and 4-GeV proton energies, a linear interpolation between corresponding CS values in the ranges (200–660) MeV and (660–2000 (4000)) MeV was done with $\Delta E_n = 1$ MeV bins. The respective calculated sums of cross sections are given in Table 6.

The results for the neutron fluxes ϕ_1, ϕ_2 and ϕ_3 calculated by formulas (7), (5) and (3), respectively, with the use of the data of Table 6 as well the experimental reaction rates from Tables 4 and 5 are given in Table 7 for $E_d = 4$ and 8 GeV.

An analysis of the data in Table 7 shows that if the deduced values of ϕ_1 depend slightly on the choice of the effective end of neutron spectrum E^{max}, so the respective fluxes ϕ_2, and especially ϕ_3, change significantly for two variants of the E^{max} choice. To choose between these options, we take into account that the calculated reaction rates R_3 for ^{7}Be production presented in Table 5 changed by less than 1% as the E^{max} value increased from 800 (1000) MeV to 2(4) GeV.
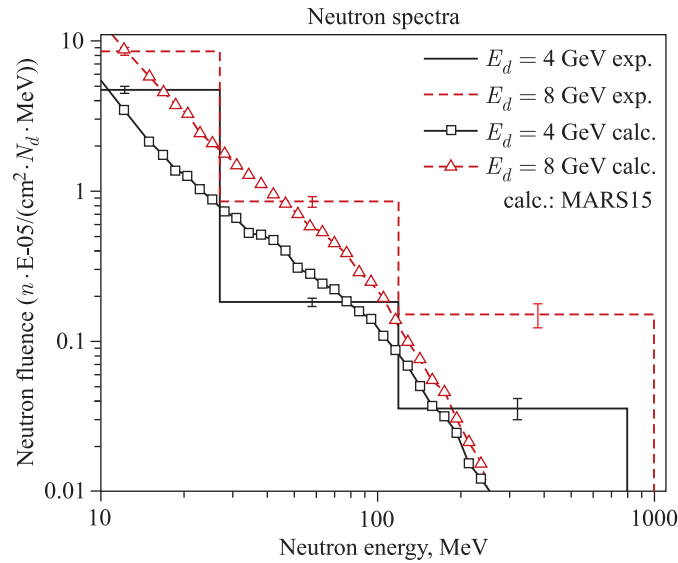

Fig. 4. The neutron fluxes as a function of three neutron energy ranges for 4- and 8-GeV beam energies

14

So, for the final values of ϕ_i(exp) we have to accept the same marked as [b] shown in Fig. 4 below.

One can see from Table 7 that if the flux ϕ_1(exp) increases about two times with growth of the deuteron energy from 4 to 8 GeV, so the ϕ_2(exp) and ϕ_3(exp) values increase in more than four times. It confirms the conclusion deduced above (see the discussion of Table 5 in Sec. 2) that the neutron spectrum in TA QUINTA becomes more "hard" with increase of incident energy. Note, that as in the case of the $^{27}\text{Al}\,(n, y_3)\,^7\text{Be}$ reaction rates, the fluxes ϕ_3(calc) reproduce neither absolute values of ϕ_3(exp) nor their dependence on deuteron energy.

4. SIMULATION OF NEUTRON SPECTRA
AND REACTION RATES AT SAMPLE POSITIONS

The calculations of the neutron spectra were performed with the use of the Monte-Carlo code MCNPX2.7 [34] combining the INCL4 intranuclear cascade model with the ABLA fission-evaporation model and cross-section libraries LA150 (up to 150 MeV) and ENDF/B-VII (up to 200 MeV). The second set of simulations was performed using the MARS15 [35, 36] code working in the MCNP mode with the neutron transport threshold set to 1E-9 MeV. The neutron production by incident deuterons in the target was modeled exclusively employing the LAQGSM [37] generator.

The geometrical and physical properties of QUINTA set-up and its materials were supplied to the code as an input deck. Such beam parameters as the displacement between axis of beam and axis of set-up (x_c, y_c) and the beam profile $(x(\text{FWHM}), y(\text{FWHM}))$ were determined from the copper activation foils [38] and the set of solid-state nuclear track detectors (SSNTD) [39], placed in the front of the set-up. The data from SSNTD were fitted by the Gaussian function $(x_c = 2.0(2)$ cm, $y_c = -0.59(5)$ cm, $x(\text{FWHM}) = 1.3(1)$ cm, $y(\text{FWHM}) = 1.61(5)$ cm for deuteron beam with the energy of 4 GeV and $x_c = 1.42(5)$ cm, $y_c = -0.18(5)$ cm, $x(\text{FWHM}) = 1.56(5)$ cm, $y(\text{FWHM}) = 2.24(5)$ cm at 8 GeV) and were used for calculations of the neutron spectra.

In order to obtain the reaction rates (R) at different positions inside TA QUINTA with the use of the MCNPX2.7 code, the simulated neutron spectra were convoluted with the cross sections of the reactions of interest. The neutron reaction cross sections for the neutron energies up to 20 MeV were taken from the TENDL-2012 data library [40], those between $E_n = 20$ MeV and $E_n = 200$ MeV were calculated by the TALYS 1.4 code [23]. Finally, above 200 MeV the cross section values were set to the same values as for $E_n = 200$ MeV.

In the MARS15 code for calculations of the nuclide yields in the samples due to interactions of neutrons with $E_n < 14$ MeV, ENDF\B-VI cross sections were used through the MCNP interface. The current realization of the model for

residual isotope production by low-energy neutrons in MARS15 does not involve the respective production cross sections. Rather it estimates which residual nucleus is produced in a particular interaction based on ENDF\B-VI cross sections of the nucleon emission using conservation laws. Such an approximation in the MARS15 code is justified by the scope of its usage in the applications that do not require a precise knowledge of the isotope production by the low-energy neutrons (although, the efforts are being undertaken to replace that model with the TENDL-2012 data library [40]). The current model is an approximation because the interactions where more than one residual nuclide is produced are not considered (in spite of that the MARS15 fission model is explicitly based on fission cross sections). That can explain the difference with the TENDL-2012-based model of the MCNPX and MARS15 results (see Table 5).

CONCLUSIONS

The experimental reaction rates for production of ^{24}Na, ^{22}Na and ^{7}Be in the ^{27}Al sample irradiated by neutrons produced in TA QUINTA when it is bombarded with deuteron beams from JINR Nuclotron have been measured in deuteron energy range (2–8) GeV.

If the ratio $\langle R \rangle \, (8 \text{ GeV}) / \langle R \rangle \, (4 \text{ GeV})$ for ^{24}Na production (having a low reaction threshold 5 MeV) is less about two, so for ^{22}Na and ^{7}Be product nuclei with much higher thresholds (25 and 119 MeV, respectively) these ratios reach about 4.7 and 4.5, correspondingly. It gives strong evidence that the neutron spectrum on the surface of TA QUINTA becomes "harder" with increase of incident energy.

At 4-GeV deuteron energy for the effective thresholds $E_{\text{th eff}} \leqslant 27$ MeV the MCNPX2.7 code reproduces $\langle R \rangle$ values rather well, while for $E_{\text{th eff}} = 119$ MeV the disagreement reaches 15 times. In the case of 8-GeV deuteron energy for highest thresholds of ^{7}Be, the exp/(calc) ratio increases up to 6.0. For the MARS15 code the situation is worse: the difference between experimental and calculated $\langle R \rangle$ values at $E_{\text{th eff}} = 119$ MeV reaches 4.4 and 20 times for the deuteron energies of 4 and 8 GeV, respectively. This means that the used codes are not able to reproduce the high-energy part of the neutron spectrum of TA QUINTA. And, moreover, the obtained results indicate their instability in the transition from one to another code.

The neutron spectrum on surface of TA QUINTA was studied using the method described in Sec. 3. The neutron flux was estimated in three ranges of neutron energy E_n corresponding to the production of ^{24}Na, ^{22}Na and ^{7}Be nuclei. An analysis of the deduced spectra and its comparison with calculation confirms in general the conclusions made just above.

REFERENCES

1. C. D. Bowman *et al.*, Nucl. Instrum. Methods. A **320**, 336 (1992).

2. F. Carminati *et al.*, CERN Report CERN/AT/93-47 (ET) (1993).

3. C. Rubbia, J. A. Rubio *et al.*, CERN Report CERN/AT/95-44 (ET) (1995).

4. C. Rubbia, AIP Conference 346, Proceedings of International Conference on Accelerator-Driven Transmutation Technologies and Applications (Las Vegas (NV), USA, 1994).

5. D. Beller, Proceedings of the OECD/NEA Eighth Information Exchange Meeting on Partitioning and Transmutation (Las Vegas (NV), USA, 2004).

6. Sakamoto Shinichi *et al.*, Nucl. Instrum. Methods. A **562**, 638 (2006); http://www.kek.jp/intrae/index.html.

7. P. Singh *et al.*, PRAMANA — Journal of Physics. **68**, 331 (2007).

8. F. Shinian *et al.*, Proceedings of SRF2011, 977, (Chicago, USA, 2011).

9. H. A. Abderrahim *et al.*, Nuclear Physics News. **20**, 24 (2010); http://www.sckcen.be/myrrha/.

10. B. Blau *et al.*, Neutron News. **20**, 5 (2009); http://sinq.web.psi.ch/.

11. G. N. Kim *et al.*, Nucl. Instrum. Methods. A **485**, 458 (2002).

12. G. Tagliente *et al.*, Brazilian Journal of Physics. **34**(3A) (2004); http://pceet075.cern.ch/.

13. J. Blomgren, PRAMANA — Journal of Physics. **68**, 269 (2007).

14. P. Bém *et al.*, Proceedings of the International Conference on Nuclear Data for Science and Technology — ND2007, p. 555 (Nice, France, 2007).

15. J. Adam *et al.*, Eur. Phys. J. A **43**, 159 (2010).

16. Chitra Bhatia *et al.*, Applied Radiation and Isotopes. **70**, 1254 (2012).

17. J. Adam *et al.*, Eur. Phys. J. A **47**, 85 (2011).

18. W. Furman, J. Adam, A. Baldin *et al.* (Baldin ISHEPP XXI) 086, JINR Dubna, September 2012; http://pos.sissa.it/cgi-bin/reader/conf.cgi?confid=173

19. www-nds.iaea.org/exfor/

20. O. Schwerer, K. Okamoto, Report INDC(NDS)-218/GZ+ (1989).

21. V. S. Barashenkov, Comp. Phys. Comm. **126**, 28 (2000).

22. V. Kumar, Chitra Bhatia, H. Kumawat, Eur. Phys. J. A **40**, 231 (2009).

23. A. J. Koning *et al.*, Nucl. Instrum. Methods. A **414**, 49 (1998); www.talys.eu.

24. J .Adam *et al.*, Eur. Phys. J. A **23**, 61 (2005).

25. J. Banaige *et al.*, Nucl. Instrum. Methods. **95**, 307 (1971).

26. P. Kozma, V. V. Yanovsky, Czech. J. Phys. **40**, 393 (1990).

27. J. Frána, J. Rad. Nucl. Chem. **257**, 583 (2003).

28. R. G. Helmer, E. Schinfeld, LNE-LNHB/CEA (2004).

29. M. Galan, LNE-LNHB/CEA (2009).

30. R. G. Helmer, E. Schinfeld, LNE-LNHB/CEA (2004).

31. L. Závorka, J. Adam *et al.* To be published.

32. G. L. Morgan *et al.*, Nucl. Instrum. Methods. B **211**, 297 (2003).

33. Yu. E. Titarenko *et al.*, Physics of Atomic Nuclei. **74**, 507 (2011).

34. D. Pelowitz, MCNPX^{TM} User's Manual, Version 2.7.0, LA-CP-11-00438 (2011).

35. N. V. Mokhov *et al.*, Technical Report FERMILAB-CONF-12-635-APC (2012); http://www-ap.fnal.gov/MARS/.

36. N. Mokhov *et al.*, accepted to Progress in Nuclear Science and Technology, FERMILAB-CONF-12-635-APC (2014).

37. S. G. Mashnik *et al.*, LANL Report LA-UR-08-2931 (2008).

38. V. Wagner *et al.*, Energy & Transmutation of RAW Workshop (Rez near Prague, Czech Republic, 2012).

39. I. Zhuk *et al.*, Energy & Transmutation of RAW Workshop (Rez near Prague, Czech Republic, 2012).

40. A. J. Koning, D. Rochman, Nucl. Data Sheets. **113**, 2841 (2012).

Редактор *В. В. Булатова*